ACS APPLIED MATERIALS & INTERFACES

Research Article

www.acsami.org

Pulsed Laser-Assisted Focused Electron-Beam-Induced Etching of Titanium with XeF_2: Enhanced Reaction Rate and Precursor Transport

J. H. Noh,[†] J. D. Fowlkes,[†,‡] R. Timilsina,[†] M. G. Stanford,[†] B. B. Lewis,[†] and P. D. Rack*[,†,‡]

[†]Department of Materials Science, Engineering, University of Tennessee, Knoxville, Tennessee 37996, United States

[‡]Center for Nanophase Materials Sciences, Oak Ridge National Laboratory, Oak Ridge, Tennessee 37831, United States

Supporting Information

ABSTRACT: In order to enhance the etch rate of electron-beam-induced etching, we introduce a laser-assisted focused electron-beam-induced etching (LA-FEBIE) process which is a versatile, direct write nanofabrication method that allows nanoscale patterning and editing. The results demonstrate that the titanium electron stimulated etch rate via the XeF_2 precursor can be enhanced up to a factor of 6 times with an intermittent pulsed laser assist. The evolution of the etching process is correlated to in situ stage current measurements and scanning electron micrographs as a function of time. The increased etch rate is attributed to photothermally enhanced Ti−F reaction and TiF_4 desorption and in some regimes enhanced XeF_2 surface diffusion to the reaction zone.

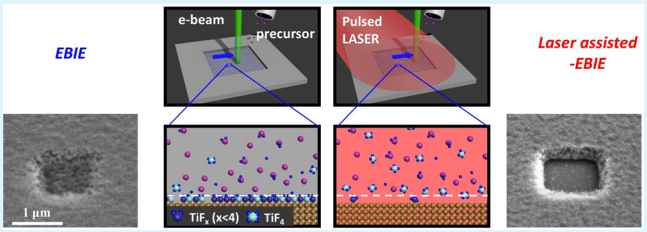

KEYWORDS: *focused electron-beam-induced etching (FEBIE), focused electron-beam-induced processing (FEBIP), laser-assisted reaction, Ti, XeF_2, nanofabrication*

INTRODUCTION

Focused electron-beam-induced etching (FEBIE) is a versatile, direct write nanofabrication method that allows nanoscale patterning and editing and is an alternative to focused ion beam (FIB) etching.[1−4] FIB etching can cause collateral subsurface damage due to knock-on collisions and ion implantation, which are major problems, for instance, in lithography mask repair and circuit editing.[5−7] In contrast, FEBIE is minimally invasive because of the low electron mass and offers high etch selectivity between different materials because it is directed via a chemical etching mechanism dependent on the precursor/substrate material combination.[8] Additionally, the FEBIE process has better spatial resolution due to the smaller beam spot size, though proximity effects recently enumerated for electron-beam-induced deposition (EBID)[9] have to be considered. FEBIE has opened up paths for high-resolution nanopatterning of materials such as photoresist, SiO_2, SiN_x, Al_2O_3, Cr, CrO_x, TaN, GaAs, and Ti by using a variety of precursor gases such as O_2, XeF_2, NOCl, and Cl_2.[4,7,10−17]

As schematically illustrated by Figure 1, the FEBIE process is governed by an electron-induced reaction with a precursor at the surface of the substrate, which results in the formation of volatile etch byproducts. Locally injected precursor molecules adsorb on the substrate surface for an average residence time, which is determined by the gas−surface interactions and the temperature of the surface (Figure 1a). Energetic primary and the subsequent secondary (SE) and backscattered electrons (BSE) interact with the adsorbed precursor molecules and result in the dissociation of the precursor molecule into radical species. These radicals subsequently react with the near-surface atoms of the solid substrate and form volatile byproducts. The resultant byproducts also have a residence time dependent on the surface temperature. Eventually, the volatile byproducts desorb from the surface and are pumped from the system. This complex process can be rate limited by different mechanisms depending on: (1) the electron and precursor parameters, (2) the electron-stimulated reaction rates, and (3) the byproduct volatility (or residence time). While continuous substrate heating can reduce the byproduct residence time, the higher temperature concomitantly decreases the reactant residence time, which can reduce the reactant equilibrium coverage and ultimately decrease the electron stimulated etching (or deposition) rate.[18,19] Conversely, cryogenic EBIE was recently shown to enhance the silicon etch rate where the low substrate temperature facilitated the residence time of the NF_3 precursor.[20] Continuous substrate heating in focused beam systems is cumbersome and can cause thermal drift and unintended reactions, for instance, interdiffusion and/or compound formation between materials. To address these problems, a pulsed laser-assisted electron-beam-induced deposition[21−23] and annealing process[24] has been recently shown to enhance byproduct desorption resulting in higher purity EBID deposits.

In this work, we explore laser-assisted focused electron-beam-induced etching. Electron-beam-induced etching of titanium with XeF_2 was recently studied,[16] and thus we use this material/precursor combination as our test case to demonstrate enhanced etch rate via a laser-assisted process. As De Teresa

Received: December 1, 2014
Accepted: January 28, 2015
Published: January 28, 2015

DOI: 10.1021/am508443s
ACS Appl. Mater. Interfaces 2015, 7, 4179−4184

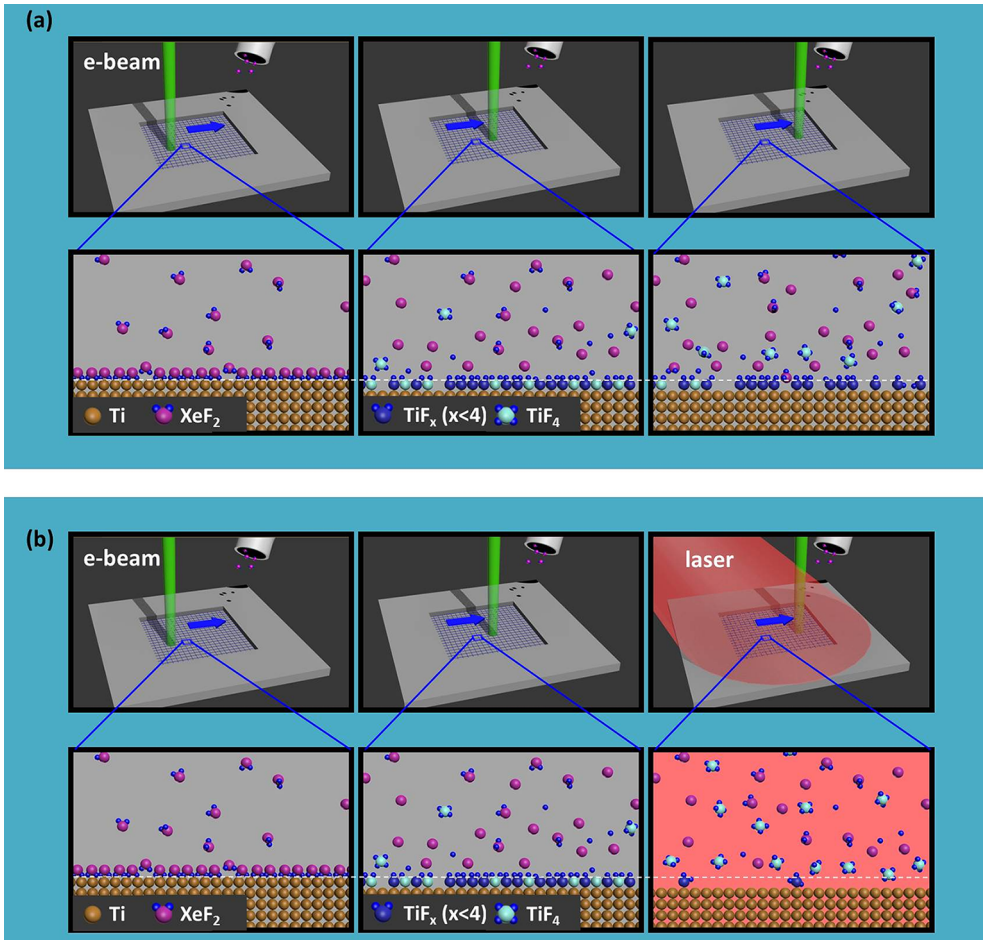

Figure 1. Schematic diagrams of (a) focused electron-beam-induced etching and (b) laser-assisted focused electron-beam-induced etching of Ti with an XeF_2 precursor. In both processes the electron beam stimulates the XeF2 dissociation which subsequently reacts and forms predominantly volatile TiF_4 species. Notably, the laser process facilitates the TiF_4 production and thus the etch rate. Not illustrated is enhanced surface diffusion transport of the precursor to the reaction zone.

et al. demonstrated, the FEBIE etch rate of Ti is strongly dependent on the electron beam parameters such as beam energy, current, dwell time, and pixel spacing.[16] The process is sensitive to the mass transport/reaction rate limited transition as well as electron-induced redissociation of the volatile byproducts, which has also been demonstrated for the XeF_2–SiO_2 etching.[4] Other relevant work on conventional fluorine-based titanium plasma etching suggests the mechanism of Ti–F etching is attributed to the reaction of fluorine radicals with titanium to form TiF_x products, where progressive fluorine incorporation drives x toward the volatile product of TiF_4.[16,25–27] Notably TiF_3 is a stable solid at room temperature.

RESULTS AND DISCUSSION

A periodic and appropriately synchronized pulsed laser can locally and briefly raise the surface temperature, which can affect the FEBIE process in several ways, where the arrows indicate whether the effect is expected to increase (↑) or decrease (↓) the FEBIE rate: enhance the *precursor* (1) surface diffusion (↑), (2) desorption (↓), (3) reaction with the substrate material (↑), and facilitate *byproduct* (4) desorption (↑) and (5) surface diffusion (↑).

A schematic diagram of the experimental setup used in this work is shown in Figure 1 and is discussed in detail elsewhere.[23] Briefly, the cycle begins when the rastered electron beam locally stimulates the dissociation of the adsorbed XeF_2 molecules and induces fluorine reactions with the titanium film to create titanium fluorides, where the final fluorine insertion (TiF_3 + F → TiF_4) is reported to be the rate-limiting step.[28] The resultant TiF_4 byproducts reside on the surface for a finite time before desorbing from the surface. The results will suggest that the intermittent laser pulse photothermally heats the surface sufficiently to (1) facilitate the TiF_4 insertion reaction and subsequent desorption (Figure 1b) and (2) enhance precursor transport to the etch region via localized surface diffusion. First, we explored the effect of electron beam dwell time on the FEBIE of Ti. Figure 2(a)–(d) shows SEM images of the Ti etch regions after 3 min of etching as a function of the electron beam dwell time. It is clearly demonstrated that etch rate decreases as electron beam dwell time increases. Consistent with De Teresa et al. the electron beam dwell time dependence on the etch rate can be attributed to the precursor depletion, which causes mass transport limited etching.[16] A second test was run with a 100 ns dwell time and an increased current of 400 and 1600 pA. Figure 2(e) and (f) compares the tilted SEM micrographs of the resultant etched features; clearly an etch retardation regime emerges in which the etch rate in the scanned area is effectively zero with an etched ring around the scanned region. The higher current regime demonstrated in Figure 2(e) and (f) is consistent with electron redissociation of

DOI: 10.1021/am508443s
ACS Appl. Mater. Interfaces 2015, 7, 4179–4184

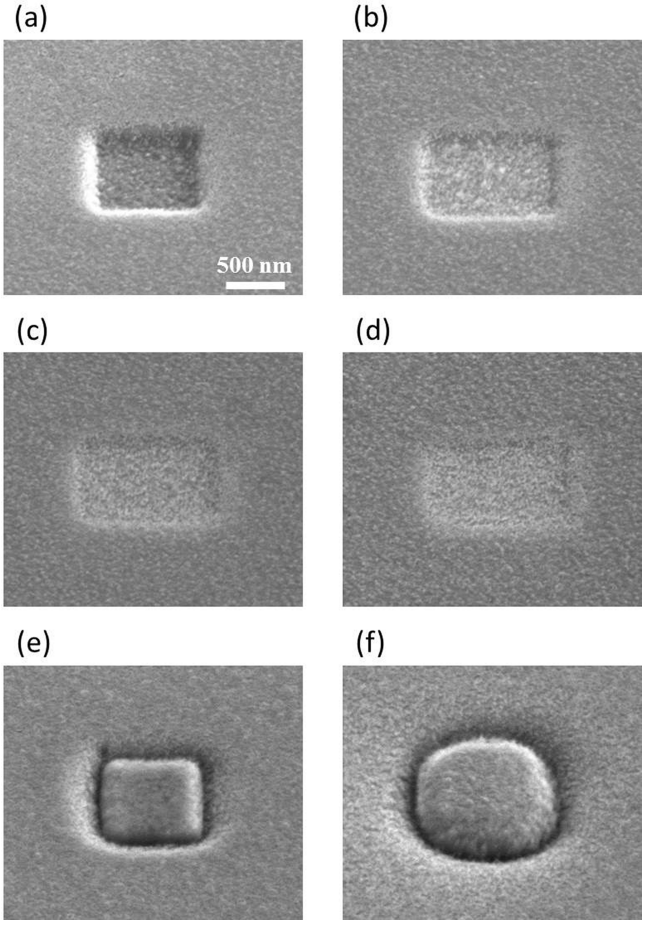

Figure 2. SEM images of the Ti etch regions after 3 min etching with 98 pA beam current and electron beam dwell times of (a) 0.1, (b) 1, (c) 10, and (d) 100 μs and with 0.1 μs electron beam dwell time and (e) 400 pA and (f) 1600 pA beam current.

TiF_4 byproducts to nonvolatile etch products (for instance $TiF_4 + e^- \rightarrow TiF_3 + F$), which forms a thin passivating layer and inhibits subsequent etching (see Supporting Information for 400 and 1600 pA − 1 μs dwell time results).[4]

Figure 3 shows simulated surface temperature transients for the 200 nm Ti/100 nm SiO_2/Si multilayered substrate. The

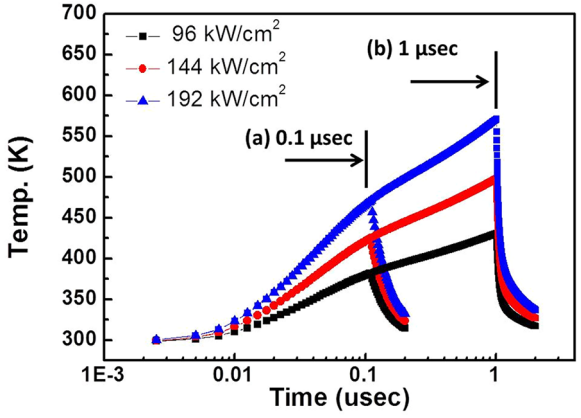

Figure 3. Simulated time−temperature plots of a 915 nm laser irradiated with (a) 0.1 and (b) 1 μs laser pulse width onto the 200 nm Ti/100 nm SiO_2/Si substrate with various energy densities.

simulation parameters are summarized in the Supporting Information, and the details of the simulation methods can be found in the Supporting Information in ref 24. As laser power (and pulse width) increases, the surface temperature increases. However, if the surface temperature is too high, pyrolytic laser-induced dissociation and etching can occur in the whole laser spot area (see Supporting Information). Thus, a critical temperature range exists in which the nanoscale focused electron beam process can be enhanced via the laser assist. The laser wavelength (915 nm or 1.36 eV) was intentionally chosen to be lower than typical bond dissociation energies, thus mitigating photolytic dissociation of the precursor.[23,29−31] Figure 4(a) compares SEM images of the FEBIE and laser-

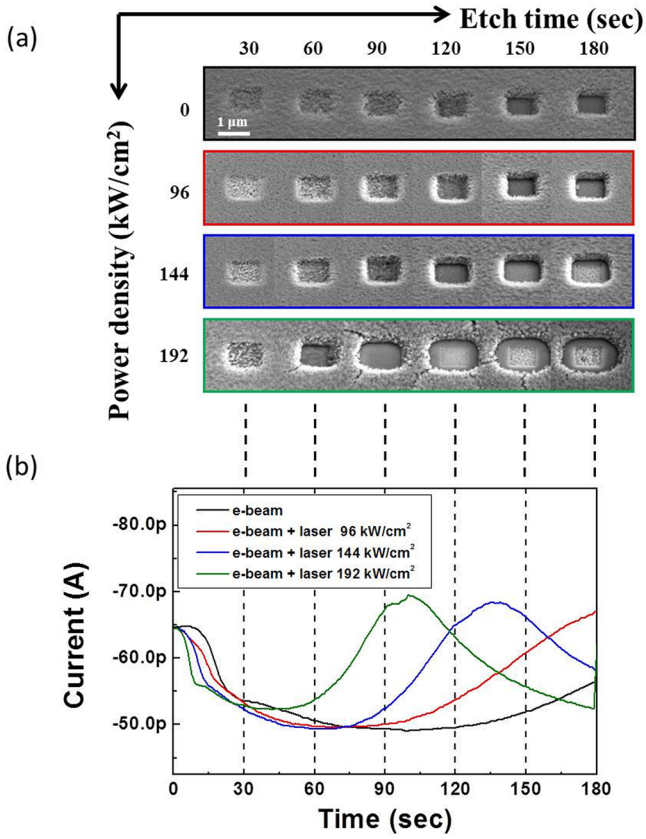

Figure 4. (a) SEM images of the laser-assisted EBIE of titanium as a function of etch time as a function of laser power density with a fixed 98 pA current and at 0.1 μs electron beam dwell time. (b) Accompanying stage current traces during etching for the 3 min etch tests.

assisted FEBIE (LA-FEBIE) of Ti as a function of laser power density and processing time. It is clearly shown that etch rate is increased with increasing laser power.

In situ stage current traces yield useful information regarding the EBIE dynamics (Figure 4(b); note the y axis is negative current). Recall that the stage current is the sum of the primary electrons (PEs) (negative), the secondary electrons (SEs) (positive), and backscattered electrons (BSEs) (positive). Several regions can be distinguished in the stage current measurements and correlated to the observed etching profiles. The initial steep decrease in the stage current magnitude (−65 to ∼−57 pA) is attributed to etching of the native TiO_2 surface layer and the development of nanoscale roughness, which increases the net SE yield. Similar stage current behavior and

DOI: 10.1021/am508443s
ACS Appl. Mater. Interfaces 2015, 7, 4179−4184

Table 1. Etching Rate and Yield as a Function of Laser Power Density with a Fixed 98 pA Current

laser power density (kW/cm^2)	0	96	144	192
etch rate (nm^3/s)	1.31×10^{16}	1.62×10^{16}	2.09×10^{16}	3.14×10^{16}
etch yield (nm^3/electron)	8.18×10^{-4}	1.01×10^{-3}	1.30×10^{-3}	1.96×10^{-3}

surface roughening were also observed in EBIE of amorphous carbon.[32] Subsequent to this region, the stage current magnitude continues decreasing to a minimum as the surface roughness and SE emission increase. Finally the stage current magnitude increases as the surface roughness decreases at the SiO_2 interface. Beyond the minimum stage current, correlation to the SEM images suggest that ~−55 pA appears to be the end point where the titanium film is completely etched and the silicon oxide underlayer surface is smooth. The stage current magnitude increases beyond this point to a maximum value where the SiO_2 surface is fully exposed and apparently has a lower combined SE and BSE yield compared to titanium. For the higher power laser-assisted etches, the current magnitude increases as the SiO_2 surface is fluorinated and develops surface roughness, and the underlying SiO_2 film is etched. Clearly each regime is accelerated with increasing laser power as the periodically pulsed laser facilitates the FEBIE process. Comparing the times of the stage current minima, the laser-assisted etch rate was improved 1.4, 1.6, and 2.4 times for the power density of 96, 144, and 192 kW/cm^2, respectively, relative to e-beam only etching. Table 1 summarizes the experimental absolute etch rates (nm^3/s) and etch yields (nm^3/electron). On the basis of the thermal simulations in Figure 3, the increased laser power periodically increases the surface temperature, and an effective activation energy was determined to be ~57 meV (see Supporting Information for an Arrhenius plot). This activation energy is much less than the estimated fluorine insertion activation energy (390 meV) and TiF_4 desorption energy (954 meV) determined for a $CF_4 + O_2$ titanium dry etch process.[28,33] We attribute the disparity in the activation energy to a relatively dilute surface concentration of fluorine, thus the process is also limited by the reactant. By comparing the laser period (10 μs) to the electron scanning parameters we note that the sample is pulsed after the electron scans ~100 pixels (~3/4 of a row in the specific ~1 μm × 1 μm experimental geometry). Interestingly, subsequent experiments were attempted with the same pulse width but longer laser periods (100 and 1000 μs), and no enhancement was observed. Thus, it appears that at longer pulse periods unreacted fluorine either diffuses away or desorbs from the electron beam/reaction zone and thus is insensitive to the laser assist.

The LAEBIE etch rate was also investigated at longer e-beam dwell times. Figure 5 compares SEM images of laser-assisted electron-beam-induced etches of Ti after 1.5 min as a function of electron beam dwell time of 0.1, 1, 10, and 100 μs. Also shown next to each SEM image is a figure illustrating the synchronization of the laser beam with the electron beam serpentine scan in a single frame where the 1 μm × 1 μm area contains 133 × 133 electron beam pixels. Interestingly, the Ti EBIE etch rate is systematically decreased as noted in Figure 2; however, the LAEBIE etch rates are all accelerated and are approximately the same (see Supporting Information for exhaustive comparison for 1, 10, and 100 μs electron beam dwell time at different laser powers and processing time). In this study, the synchronization of the laser pulse and the electron beam scanning is very different and suggests that in addition to enhancing the fluorine insertion and TiF_4 desorption the laser assist also facilitates precursor transport to the reaction zone. The progressively longer electron beam dwell times (100 ns to 100 μs) and constant laser pulse width (100 ns) and period (10 μs) significantly change the laser assist dynamics, namely, the ratio of 100/1 electron pixels/laser pulse transitions to 10 laser pulses/electron pixel! Without the laser assist, the XeF_2 adsorbed on the surface during the electron beam refresh time (i.e., the time it takes to scan all the pixels, which ranges from 1.8 ms to 1.8 s, for the 100 ns to 100 μs electron dwell times, respectively) is depleted by the electron-stimulated dissociation, and the precursor readsorption during

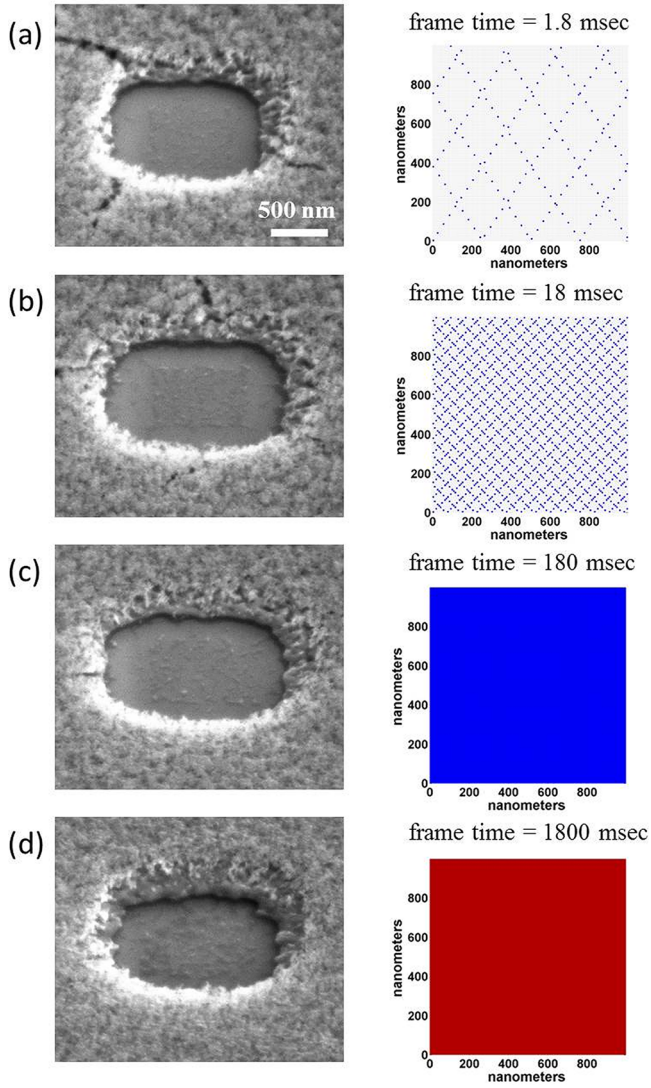

Figure 5. SEM images of the LAEBIE of Ti at 192 kW/cm^2 after 1.5 min etching with the current dwell time of (a) 0.1, (b) 1, (c) 10, and (d) 100 μs. Complementary images illustrates for each condition how the serpentine electron beam raster and flood laser pulses are synchronized during a single electron beam frame (blue denotes a single pulse, and red indicates 10 pulses). Note that each laser pulse irradiates the entire scanned area simultaneously, whereas the electron irradiates individual pixels.

DOI: 10.1021/am508443s
ACS Appl. Mater. Interfaces 2015, 7, 4179−4184

the electron beam dwell time is low. Thus, we observed the mass transport limited decrease in etching rate for the longer electron beam dwell times noted above. Conversely, the LAEBIE etch rate is accelerated for all the electron dwell times, and we suggest that the precursor mass transport is enhanced via a thermally assisted surface diffusion. While the EBIE etch studies were not fully etched in the 3 min etch time, a comparison of the stage current signatures suggests an enhancement of >6 times for the 100 μs electron beam dwell time and 192 kw/cm^2 LAEBIE processes. Future studies will be performed to investigate the anticipated competition between XeF_2 desorption and surface diffusion, which would decrease and increase a precursor-limited etch rate, respectively.

Peripheral etching beyond the scanned electron region occurs in the standard EBIE patterns and, as is well-documented in the EBIE and EBID literature, is attributed to BSE and SEII electrons. During LAEBIE, peripheral etching is also observed regardless of dwell time, as shown in Figures 4 and 5. The enhanced lateral etching is attributed to thermally assisted etching caused by BSE and SEII electrons; for instance, the same mechanisms proposed occur in this low-electron flux region. Furthermore, the lateral extent increases during the etch because SE and BSE trajectories are larger in SiO_2 relative to Ti (see Supporting Information for Monte Carlo simulations). Importantly, the stage current monitoring, as shown in Figure 4, can be used to accurately end-point the etch and minimize overetching which can exacerbate the peripheral etching and low fidelity pattern transfer.

Finally, we address the role that enhanced sublimation or desorption of TiF_3 could be contributing to the LAEBIE process. While initially we believed this mechanism could also be operative, a study at higher current revealed that, similar to the EBIE process demonstrated in Figure 2(e) and (f), the LABIE process was also arrested in the scanned beam area for the laser conditions studied (see Supporting Information). As suggested above, the high-current zero EBIE etch rate is consistent with the subsequent electron stimulated reaction $TiF_4 + e^- \rightarrow TiF_3 + F$; this is consistent with De Teresa's high-current results[16] as well as our previous experimental and simulation study of SiO_2 etching.[4] The high-current LABIE results suggest that the resultant TiF_3 forms a passivating film, which also retards the laser assist process. Thus, we conclude that TiF_3 sublimation or desorption is not contributing to the LAEBIE.

SUMMARY

Summarily, we demonstrate a laser-assisted electron-beam-induced etching process of Ti with the XeF_2 precursor. At optimized laser conditions, below pyrolytic dissociation and etching, the pulsed laser enhances the TiF_4 reaction and desorption and thus increases the etch rate up to 2.4 times. Longer electron beam dwell time studies demonstrate that in addition to the enhanced reaction the laser assist also facilitates the precursor transport to the reaction zone, which is attributed to enhanced XeF_2 surface diffusion at elevated temperatures. The outlook for LAEBIE is extremely positive as we envision that the process will open up the possibility of selectively etching a wide variety of materials previously not volatile enough to be etched without focused ion beams. Additionally, the historically low EBIE etch rate has also been a limiting factor in high-throughput milling applications. As discussed, focused ion beam damage precludes the focused ion beam use in many applications; thus, the laser assist demonstrated here opens up the prospect that damage-free and high-rate nanoscale electron-beam-induced etching may be applied across many more applications.

METHODS

A 200 nm thick Ti layer was deposited by electron beam evaporation onto a Si substrate coated with a 100 nm thermally grown SiO_2 layer. All electron-beam-induced etching experiments were performed using an FEI Nova 600 dual beam scanning electron/ion microscope (SEM/FIB) equipped with a gas injection system (GIS), a plasma cleaner (XEI Scientific, Inc., Evactron Decontaminator), and a laser delivery probe (Oxford Instruments, Omniprobe). Prior to the etching experiments, the samples and chamber were cleaned using the plasma cleaner at a background pressure of 5.3×10^{-1} mbar using ambient air for 20 min. XeF_2 was used as the etching precursor. The temperature of the GIS was kept constant at 28 °C, and the chamber pressure was typically $\sim 5 \times 10^{-6}$ mbar during the XeF_2 exposure. The gas nozzle of the GIS was positioned ~100 μm away from the sample surface in the z direction and about 300 μm away from the sample center in order to minimize interference with the laser delivery system. The typical electron beam voltage and current were 5 keV and 98 pA, respectively. The pattern footprint was controlled by the FEI internal patterning software to be 1×1 μm^2 and scanned in a serpentine scanning strategy with a pixel pitch of 7.46 nm (50% pixel overlap). The electron beam dwell time was varied from 0.1 to 100 μs. A fiber-pigtailed 915 nm 25 W multichip diode laser module (Oclaro, BMU25B-915-01) was driven by a pulsed diode laser driver (IXYS Colorado/Directed Energy, PCX-7410). Laser pulse frequency, pulse width, and duty cycle were 100 kHz, 0.1 μs, and 1%, respectively. On the basis of the laser efficiency (~40%) and laser probe throughput (~68.5%) and ~100 μm diameter laser spot, the incident laser power density was varied from ~96 to 192 kW/cm^2. The resultant features were examined via normal and tilted (52°) SEM imaging. During etching, complementary in situ stage current measurements were performed to correlate signatures of the etching process.

ASSOCIATED CONTENT

Supporting Information

S1: EBIE results of higher e-beam current with 1 μs dwell time, S2: parameters used in the thermal simulation, S3: pyrolytic dissociation and laser-induced etching with high laser energy, S4: normalized etch rate versus (simulated maximum T)$^{-1}$ Arrhenius plot, S5: laser assisted FEBIE (LA-FEBIE) of Ti as a function of electron beam dwell time, laser power density, and processing time, S6: Monte Carlo simulations of primary and backscattered electron trajectories. This material is available free of charge via the Internet at http://pubs.acs.org.

AUTHOR INFORMATION

Corresponding Author

*E-mail: prack@utk.edu.

Notes

The authors declare no competing financial interest.

ACKNOWLEDGMENTS

The authors acknowledge that this research was conducted at the Center for Nanophase Materials Sciences, which is a DOE Office of Science User Facility. MGS acknowledges support from the National Defense Science and Engineering Graduate Fellowship funded through the AFOSR. BBL acknowledges support via the University of Tennessee Chancellor's Fellowship program. PDR and JDF acknowledge that their contributions (mentoring, design of experiments, modeling, and manuscript preparation) were supported by the Center for

DOI: 10.1021/am508443s
ACS Appl. Mater. Interfaces 2015, 7, 4179−4184

Nanophase Materials Sciences which is a DOE Office of Science User Facility.

REFERENCES

(1) Randolph, S. J.; Fowlkes, J. D.; Rack, P. D. Focused, Nanoscale Electron-Beam-Induced Deposition and Etching. *CRC Crit. Rev. Solid State Sci.* **2006**, *31*, 55−89.

(2) Utke, I.; Hoffmann, P.; Melngailis, J. Gas-Assisted Focused Electron Beam and Ion Beam Processing and Fabrication. *J. Vac. Sci. Technol., B: Nanotechnol. Microelectron.: Mater., Process., Meas., Phenom.* **2008**, *26*, 1197−1276.

(3) van Dorp, W. F.; Hagen, C. W. A Critical Literature Review of Focused Electron Beam Induced Deposition. *J. Appl. Phys.* **2008**, *104*, 081301.

(4) Lassiter, M. G.; Rack, P. D. Nanoscale Electron Beam Induced Etching: A Continuum Model that Correlates the Etch Profile to the Experimental Parameters. *Nanotechnology* **2008**, *19*, 455306.

(5) Liang, T.; Stivers, A.; Livengood, R.; Yan, P.-Y.; Zhang, G.; Lo, F.-C. Progress in Extreme Ultraviolet Mask Repair using a Focused Ion Beam. *J. Vac. Sci. Technol., B: Nanotechnol. Microelectron.: Mater., Process., Meas., Phenom.* **2000**, *18*, 3216−3220.

(6) Nishiyama, Y.; Amano, T.; Shigemura, H.; Terasawa, T.; Suga, O.; Kozakai, T.; Kikuchi, S.; Shiina, K.; Yasaka, A.; Hagiwara, R. Damage Analysis of EUV Mask under Ga Focused Ion Beam Irradiation. *Proc. SPIE* **2008**, *7028*, 70280J.

(7) Jianhua, W.; Griffis, D. P.; Garcia, R.; Russell, P. E. Etching Characteristics of Chromium Thin Films by an Electron Beam Induced Surface Reaction. *Semicond. Sci. Technol.* **2003**, *18*, 199.

(8) Toth, M. Advances in Gas-Mediated Electron Beam-Induced Etching and Related Material Processing Techniques. *Appl. Phys. A: Mater. Sci. Process.* **2014**, *117*, 1623−1629.

(9) Plank, H.; Smith, D. A.; Haber, T.; Rack, P. D.; Hofer, F. Fundamental Proximity Effects in Focused Electron Beam Induced Deposition. *ACS Nano* **2011**, *6*, 286−294.

(10) Rack, P. D.; Randolph, S.; Deng, Y.; Fowlkes, J.; Choi, Y.; Joy, D. C. Nanoscale Electron-Beam-Stimulated Processing. *Appl. Phys. Lett.* **2003**, *82*, 2326−2328.

(11) Randolph, S. J.; Fowlkes, J. D.; Rack, P. D. Focused Electron-Beam-Induced Etching of Silicon Dioxide. *J. Appl. Phys.* **2005**, *98*, 034902.

(12) Yemini, M.; Hadad, B.; Liebes, Y.; Goldner, A.; Ashkenasy, N. The Controlled Fabrication of Nanopores by Focused Electron-Beam-Induced Etching. *Nanotechnology* **2009**, *20*, 245302.

(13) Bret, T.; Afra, B.; Becker, R.; Hofmann, T.; Edinger, K.; Liang, T.; Hoffmann, P. Gas Assisted Focused Electron Beam Induced Etching of Alumina. *J. Vac. Sci. Technol., B: Nanotechnol. Microelectron.: Mater., Process., Meas., Phenom.* **2009**, *27*, 2727−2731.

(14) Wang, S.; Sun, Y.-M.; White, J. M.; Stivers, A.; Liang, T. Electron-Beam-Assisted Etching of CrOx Films by Cl_2. *J. Vac. Sci. Technol., B: Nanotechnol. Microelectron.: Mater., Process., Meas., Phenom.* **2005**, *23*, 206−209.

(15) Ganczarczyk, A.; Geller, M.; Lorke, A. XeF_2 Gas-Assisted Focused-Electron-Beam-Induced Etching of GaAs with 30 nm Resolution. *Nanotechnology* **2011**, *22*, 045301.

(16) Schoenaker, F. J.; Cordoba, R.; Fernandez-Pacheco, R.; Magen, C.; Stephan, O.; Zuriaga-Monroy, C.; Ibarra, M. R.; De Teresa, J. M. Focused Electron Beam Induced Etching of Titanium with XeF_2. *Nanotechnology* **2011**, *22*, 265304.

(17) Lassiter, M. G.; Liang, T.; Rack, P. D. Inhibiting Spontaneous Etching of Nanoscale Electron Beam Induced Etching Features: Solutions for Nanoscale Repair of Extreme Ultraviolet Lithography Masks. *J. Vac. Sci. Technol., B: Nanotechnol. Microelectron.: Mater., Process., Meas., Phenom.* **2008**, *26*, 963−967.

(18) Mulders, J. J. L.; Belova, L. M.; Riazanova, A. Electron Beam Induced Deposition at Elevated Temperatures: Compositional Changes and Purity Improvement. *Nanotechnology* **2011**, *22*, 055302.

(19) Bishop, J.; Lobo, C. J.; Martin, A.; Ford, M.; Phillips, M.; Toth, M. Role of Activated Chemisorption in Gas-Mediated Electron Beam Induced Deposition. *Phys. Rev. Lett.* **2012**, *109*, 146103.

(20) Charlene, J. L.; Aiden, M.; Matthew, R. P.; Milos, T. Electron Eeam Induced Chemical Dry Etching and Imaging in Gaseous NH_3 Environments. *Nanotechnology* **2012**, *23*, 375302.

(21) Roberts, N. A.; Fowlkes, J. D.; Magel, G. A.; Rack, P. D. Enhanced Material Purity and Resolution via Synchronized Laser Assisted Electron Beam Induced Deposition of Platinum. *Nanoscale* **2013**, *5*, 408−415.

(22) Roberts, N. A.; Gonzalez, C. M.; Fowlkes, J. D.; Rack, P. D. Enhanced By-Product Desorption via Laser Assisted Electron Beam Induced Deposition of $W(CO)_6$ with Improved Conductivity and Resolution. *Nanotechnology* **2013**, *24*, 415301.

(23) Roberts, N. A.; Magel, G. A.; Hartfield, C. D.; Moore, T. M.; Fowlkes, J. D.; Rack, P. D. In Situ Laser Processing in a Scanning Electron Microscope. *J. Vac. Sci. Technol., A* **2012**, *30*, 041404.

(24) Stanford, M. G.; Lewis, B. B.; Noh, J. H.; Fowlkes, J. D.; Roberts, N.; Plank, H.; Rack, P. Purification of Nanoscale Electron Beam Induced Platinum Deposits via Pulsed Laser Induced Oxidation Reaction. *ACS Appl. Mater. Interfaces* **2014**, *6*, 21256−21263.

(25) Yu, M. L.; Ahn, K. Y.; Joshi, R. V. Surface Reactions in the Chemical Vapor Deposition of Tungsten using WF_6 and SiH_4 on Al, PtSi, and TiN. *J. Appl. Phys.* **1990**, *67*, 1055−1061.

(26) Haendler, H. M.; Bartram, S. F.; Becker, R. S.; Bernard, W. J.; Bukata, S. W. The Reaction of Fluorine with Titanium, Zirconium and the Oxides of Titanium(IV), Zirconium(IV) and Vanadium(V). *J. Am. Chem. Soc.* **1954**, *76*, 2177−2178.

(27) Ramanath, G.; Greene, J. E.; Carlsson, J. R. A.; Allen, L. H.; Hornback, V. C.; Allman, D. J. W Deposition and Titanium Fluoride Formation during WF_6 Reduction by Ti: Reaction Path and Mechanisms. *J. Appl. Phys.* **1999**, *85*, 1961−1969.

(28) Fracassi, F.; d'Agostino, R. Chemistry of Titanium Dry Etching in Fluorinated and Chlorinated Gases. *Pure Appl. Chem.* **1992**, *64*, 703−707.

(29) Hwang, D. J.; Misra, N.; Grigoropoulos, C. P.; Minor, A. M.; Mao, S. S. In Situ Monitoring of Material Processing by a Pulsed Laser Beam Coupled via a Lensed Fiber into a Scanning Electron Microscope. *J. Vac. Sci. Technol., A* **2008**, *26*, 1432−1438.

(30) Herman, I. P. Laser-Assisted Deposition of Thin Films from Gas-Phase and Surface-Adsorbed Molecules. *Chem. Rev.* **1989**, *89*, 1323−1357.

(31) Turney, W.; Hung, Y. M.; Starcevich, S. G.; Cardinahl, P. S.; Grassian, V. H.; Singmaster, K. A. Pulsed Laser-Assisted Chemical Vapor Deposition of Tungsten, Molybdenum, and Vanadium Thin Films. *Chem. Mater.* **1992**, *4*, 1192−1199.

(32) Miyazoe, H.; Utke, I.; Michler, J.; Terashima, K. Controlled Focused Electron Beam-Induced Etching for the Fabrication of Sub-Beam-Size Nanoholes. *Appl. Phys. Lett.* **2008**, *92*, 043124.

(33) Ranta, M. Dry Etching of Titanium. *Symp. Proc. - Int. Symp. Plasma Chem., 7th* **1985**, 954.

DOI: 10.1021/am508443s
ACS Appl. Mater. Interfaces 2015, 7, 4179−4184